related transcriptional errors leading to mutant proteins could result in "error catastrophe" where genes necessary for cellular viability become compromised, resulting in age-related cell death (*28*). This mechanism may also provide one explanation for adaptive (or directed) mutagenesis (*29*). Future studies should be focused on determining the extent to which transcriptional base substitution contributes to the mutant protein burden of cells.

References and Notes

1. H. Echols and M. F. Goodman, *Mutat. Res.* **236**, 301 (1990); L. A. Loeb and B. D. Preston, *Annu. Rev. Genet.* **20**, 201 (1986).
2. H. Maki and M. Sekiguchi, *Nature* **355**, 273 (1992).
3. B. K. Duncan and J. H. Miller, *ibid.* **287**, 560 (1980).
4. I. Mellon *et al.*, *Science* **272**, 557 (1996); C. P. Selby and A. Sancar, *ibid.* **260**, 53 (1993).
5. I. Mellon *et al.*, *Proc. Natl. Acad. Sci. U.S.A.* **83**, 8878 (1986); I. Mellon, G. Spivak, P. C. Hanawalt, *Cell* **51**, 241 (1987); P. K. Cooper, T. Nouspikel, S. G. Clarkson, S. A. Leadon, *Science* **275**, 990 (1997); S. A. Leadon and P. K. Cooper, *Proc. Natl. Acad. Sci. U.S.A.* **90**, 10499 (1993).
6. P. Doetsch *et al.*, in *DNA Damage and Repair: Oxygen Radical Effects, Cellular Protection, and Biological Consequences*, M. Dizdaroglu, Ed. (Plenum, New York, 1998), pp. 97–110.
7. W. Zhou and P. W. Doetsch, *Proc. Natl. Acad. Sci. U.S.A.* **90**, 6601 (1993).
8. A. Viswanathan and P. W. Doetsch, *J. Biol. Chem.* **273**, 21276 (1998).
9. J. Liu, W. Zhou, P. W. Doetsch, *Mol. Cell. Biol.* **15**, 6729 (1995).
10. J. Liu and P. W. Doetsch, *Nucleic Acids Res.* **26**, 1707 (1998).
11. Y. H. Chen and D. F. Bogenhagen, *J. Biol. Chem.* **268**, 5849 (1993).
12. B. A. Bridges, *Cancer Surv.* **28**, 155 (1996).
13. J. Gallant and L. Palmer, *Mech. Ageing Dev.* **10**, 27 (1979).
14. F. Taddei *et al.*, *Science* **278**, 128 (1997).
15. E. C. Friedberg, G. C. Walker, W. Siede, *DNA Repair and Mutagenesis* (ASM Press, Washington, DC, 1995).
16. pBest-luc, an *E. coli* tac-luciferase expression plasmid was obtained from Promega (Madison, WI). This plasmid was cut at unique sites with Cla I (1373) and Pac I (1329) to replace the 45-bp segment with a synthetic, modified fragment (Cla I–Pac I fragment; template strand 5′-CGATTCCAATTCAGCGGGGGCCACCTGATATCCTTXG-TATTTAAT-3′; X is T, A, or U for Luc-WT, Luc-STOP, and Luc-U constructs, respectively). The Cla I–Pac I duplex fragment was generated by annealing the appropriate synthetic template strand with the wild-type or stop codon–containing, complementary strand, phosphorylated oligonucleotides (Gibco-BRL Life Technologies, Palo Alto, CA). The placement of uracil at the correct nucleotide position was verified by treatment of the synthetic, end-labeled Cla I–Pac I fragment with purified uracil-DNA glycosylase (Epicenter Technologies) and *E. coli* endonuclease IV (gift from R. P. Cunningham), which generated the appropriate DNA cleavage product when analyzed on a DNA sequencing gel. Five hundred micrograms of purified linear vector was used in a ligation reaction with 8 μg of the Cla I–Pac I fragment containing either a wild-type, stop, or uracil codon. The resulting Luc-WT, Luc-STOP, and Luc-U constructs were expressed in *E. coli ung*$^+$, *ung*$^-$, *mutS*$^+$, and *mutS*$^-$ cells by electroporation of 50 ng of DNA.
17. G. B. Sala-Newby and A K. Campbell, *Biochim. Biophys. Acta* **1206**, 155 (1994).
18. I. W. Althaus *et al.*, *Biochem. Pharmacol.* **51**, 1373 (1996).
19. D. M. DeMarini and B. K. Lawrence, *Mutat. Res.* **267**, 1 (1992).
20. M. Gellert *et al.*, *Proc. Natl. Acad. Sci. U.S.A.* **73**, 4474 (1976).
21. DNA synthesis was determined by pulse labeling as previously described (*30*). Briefly, at 0, 20, 60, 120, and 240 min after electroporation of Luc-WT, Luc-STOP, or Luc-U into cells, 0.4-ml portions of bacterial culture were pulsed with 2 μCi of [^{3}H-methyl]thymidine (Amersham; 75.0 Ci/mmol) for 5 min. The reaction was stopped by adding an equal volume of 10% trichloroacetic acid (TCA) to cells and holding on ice for 30 min. TCA precipitates were collected on 0.45-μm Millipore GF/A filters and rinsed with 5% TCA. The filters were dried and counted in a Wallac 1409 scintillation counter (Gaithersburg, MD). Growth-inhibited cultures [LB-novobiocin (50 μM)] were compared with growing cultures (LB alone) (*19*). The amount of novobiocin used for non-growth conditions was titrated to 50 μM, which was found to completely inhibit DNA synthesis but allowed RNA synthesis and expression of luciferase. RNA synthesis was determined by pulse labeling as previously described with slight modifications (*31*). As described above for the DNA synthesis measurements, after electroporation of Luc-WT, Luc-STOP, or Luc-U constructs into cells, 0.4-ml portions of bacterial culture were pulsed with 2 μCi of [5-^{3}H]uridine (Amersham; 25 to 30 Ci/mmol) for 5 min at the same time points used in the DNA synthesis experiments. Ten percent TCA was added to stop the reaction, which was then held on ice for 30 min. Precipitates were collected on 0.45-μm Millipore GF/A filters and rinsed with 5% TCA. The filters were dried and counted. Growth-inhibited cultures [LB-novobiocin (50 μM)] were compared with rifampicin-treated cultures [LB-rifampicin (150 μg/mL)] and growing cultures (LB alone).
22. Competent *E. coli* cells were electroporated with DNA and incubated at 37°C in 1 ml of LB media in the presence or absence of novobiocin. Optical density (600 nm) measurements to determine cell growth were conducted at 0 to 240 min after IPTG induction by removing 100 μl and diluting the cells to 1 ml in LB media.
23. I. D. Nicholl, K. Nealon, M. K. Kenny, *Biochemistry* **36**, 7557 (1997); M. Sandigursky, G. A. Freyer, W. A. Franklin, *Nucleic Acids Res.* **26**, 1282 (1998); E. Seeberg, L. Eide, M. Bjoras, *Trends Biochem. Sci.* **20**, 391 (1995); D. G. Vassylyev and K. Morikawa, *Structure* **4**, 1381 (1996).
24. G. Dianov and T. Lindahl, *Curr. Biol.* **4**, 1069 (1994).
25. B. Kramer, W. Kramer, H. J. Fritz, *Cell* **38**, 879 (1984).
26. R. S. Harris *et al.*, *Genes Dev.* **11**, 2426 (1997).
27. F. W. van Leeuwen *et al.*, *Science* **279**, 242 (1998).
28. L. E. Orgel, *Proc. Natl. Acad. Sci. U.S.A.* **49**, 517 (1963).
29. B. A. Bridges, *Nature* **375**, 741 (1995); J. Cairns, J. Overbaugh, S. Miller, *ibid.* **335**, 142 (1988); F. W. Stahl, *ibid.*, p. 112.
30. M. Kato *et al.*, *Biol. Pharm. Bull.* **16**, 552 (1993).
31. M. Yamaguchi and S. Ueoka, *Mol. Cell. Biochem.* **173**, 169 (1997).
32. After electroporation of Luc-WT, Luc-STOP, and Luc-U constructs, bacteria were incubated in LB-novobiocin (50 μM) media for 30 min and then subsequently induced with IPTG for 240 min. After the induction period, cells were harvested and placed in a luciferase lysis buffer [25 mM tris-phosphate (pH 7.8), 2 mM dithiothreitol, 2 mM 1,2-diaminocyclohexane-*N*,*N*,*N*′,*N*′-tetraacetic acid, 10% glycerol, and 1% Triton X-100] and lysed by freeze-thawing five times. The assay for luciferase activity was performed with the Luciferase Assay Kit (Promega), according to the manufacturer's instructions. Transformation efficiency (number of colonies per microgram of DNA) was calculated as the number of Amp^R colonies per microgram of DNA and was subsequently used to normalize luciferase activity values obtained for each strain used in these studies. *Escherichia coli ung*$^+$ (BW313) and *ung*$^-$ (BW312) cells were obtained from B. Weiss. *Escherichia coli mutS*$^-$ (ES1301) was obtained from the *E. coli* stock center of Yale University (New Haven, CT). *Escherichia coli mutS*$^+$ (ES943) was obtained from E. Siegal.

33. We thank G. Shadel and Y. W. Kow for critically reading this manuscript. This work was supported by NIH grants CA73041 and CA78622. A.V. was supported by the Medical Scientist Training Program at Emory University. H.J.Y. was supported by Chosun University (Republic of Korea) and the KOSEF postdoctoral fellowship program.

21 December 1998; accepted 5 March 1999

Dynamic Control of CaMKII Translocation and Localization in Hippocampal Neurons by NMDA Receptor Stimulation

Kang Shen and Tobias Meyer*

Calcium-calmodulin–dependent protein kinase II (CaMKII) is thought to increase synaptic strength by phosphorylating postsynaptic density (PSD) ion channels and signaling proteins. It is shown that *N*-methyl-D-aspartate (NMDA) receptor stimulation reversibly translocates green fluorescent protein–tagged CaMKII from an F-actin–bound to a PSD-bound state. The translocation time was controlled by the ratio of expressed β-CaMKII to α-CaMKII isoforms. Although F-actin dissociation into the cytosol required autophosphorylation of or calcium-calmodulin binding to β-CaMKII, PSD translocation required binding of calcium-calmodulin to either the α- or β-CaMKII subunits. Autophosphorylation of CaMKII indirectly prolongs its PSD localization by increasing the calmodulin-binding affinity.

CaMKII is involved in synaptic plasticity (*1*) and in the maintenance of the dendritic architecture (*2*). These different postsynaptic and dendritic functions of CaMKII make this enzyme a good model to investigate if and how signaling proteins are recruited to their sites of action. We studied the translocation of CaMKII isoforms by monitoring green fluorescent protein (GFP)–tagged CaMKII isoforms in cultured hippocampal CA1-CA3 neurons (*3*). GFP–α-CaMKII was uniformly distributed in the cell body and main processes of living neurons [Fig. 1A, (I)]. Glutamate stimulation induced a rapid enrichment of fluorescence in punctate structures along the dendritic processes and somatic cortex [Fig. 1A, (II)]

(n = 32) (*4*). Alternatively, 10-s electric field stimuli of 50 Hz also triggered GFP-CaMKII translocation to similar punctate sites (*5*). The CaMKII translocation sites were likely in postsynaptic terminals, since they correlated with cross-points of transfected dendrites and untransfected neurites. Panel III of Fig. 1A shows an overlay of a fluorescence image of GFP–α-CaMKII (green) and a differential interference contrast (DIC) image before glutamate stimulation. The sites of GFP–α-CaMKII translocation can be visualized in a difference image (red, panel IV) by subtracting the fluorescence image before glutamate stimulation from the image after stimulation.

What are these punctate dendritic target sites? Because previous biochemical studies suggested that CaMKII is associated with postsynaptic densities (PSDs) and enriches in PSD fractions during ischemic conditions or tetraethylammonium stimulation protocols (*6*), we compared the localization of GFP–α-CaMKII to that of the PSD marker PSD-95 (Fig. 1B) (*7*). The punctate distribution of GFP–α-CaMKII after glutamate stimulation (green) showed a marked colocalization with antibodies to PSD-95 (red) (n = 7), suggesting that CaMKII translocates to PSD. A similar colocalization was observed between GFP–α-CaMKII and FM 4-64, a marker for functional presynaptic terminals juxtaposed to PSD (*4*). Together, these results suggest that GFP–α-CaMKII translocates to PSDs after glutamate or electrical stimulation.

The localization of GFP–α-CaMKII to PSD is a Ca^{2+}-dependent process, because the translocation could readily be reversed by chelating extracellular Ca^{2+} concentrations after glutamate addition. Panels I and II of Fig. 1C show the glutamate-triggered PSD translocation of GFP-CaMKII, while panel III shows the reversal by lowering extracellular Ca^{2+}. Panel IV shows that the translocation to PSD could be repeated by subsequent addition of glutamate and extracellular Ca^{2+}. This glutamate-induced translocation was repeatable at least four times (n = 3) (*5*). These findings not only show that the translocation of CaMKII is a Ca^{2+}-mediated process but also suggest that PSD translocation is a dynamic state of CaMKII that reversibly enhances the phosphorylation of PSD-localized substrates.

Although the α isoform of CaMKII has been extensively studied, much less is known about β-CaMKII. We recently reported that β-CaMKII can bind to F-actin in vitro and colocalizes with F-actin in vivo when expressed in different cell types. Coexpression of β- and α-CaMKII leads to the formation of large hetero-oligomers which bind to F-actin (*8*). This F-actin localization of GFP–β-CaMKII can be seen in Fig. 2A (left). Glutamate stimulation triggered a rapid dissociation of GFP–β-CaMKII from F-actin and led to a nearly uniform cytosolic distribution of the kinase (Fig. 2A, middle). In a subsequent step, GFP–β-CaMKII translocated from the cytosol to PSD (Fig. 2A, right) (n = 22). The same F-actin dissociation and PSD translocation of CaMKII hetero-oligomers was also observed when GFP–α-CaMKII was expressed in the same neurons together with β-CaMKII (*5*).

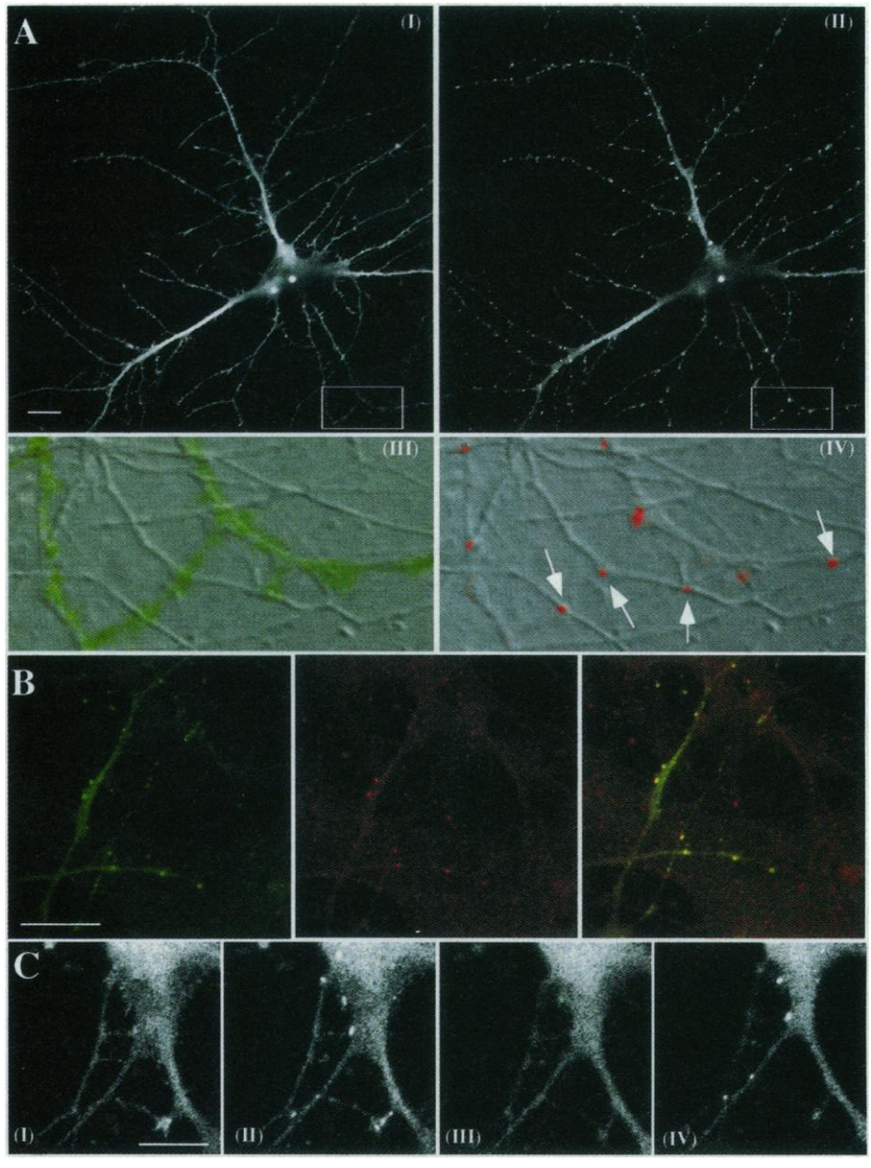

Fig. 1. Glutamate-induced translocation of α-CaMKII to PSD. (**A**) (panel I) GFP–α-CaMKII–transfected CA3-CA1 neurons (12 days in culture) showed a uniform cytosolic fluorescence distribution. In panel II, the same neuron is shown after stimulation with 100 μM glutamate plus 10 μM glycine. A marked translocation of GFP–α-CaMKIIα to local sites can be observed after 20 s. Panel III shows an overlay of a DIC image and a fluorescence image of a neuron expressing GFP–α-CaMKII before glutamate stimulation (green). Panel IV shows the translocation to punctate sites using a subtraction analysis (red; the fluorescence image after glutamate addition was subtracted from the fluorescence image before addition). Arrows point to local sites where transfected dendrites make physical contacts with untransfected neurites. (**B**) Colocalization of GFP–α-CaMKII (left, green) with antibodies to the PSD marker PSD-95 (middle, red). Colocalization is apparent as a yellow color in the merged image (right). (**C**) (panel I) GFP–α-CaMKII transfected CA1-CA3 neuron before glutamate addition. In panel II, the same neuron is shown 20 s later after addition of 50 μM glutamate plus 5 μM glycine. In panel III, the same neuron is shown 2 min later, after the extracellular buffer was exchanged to a low Ca^{2+} solution without glutamate. In panel IV, the same neuron is shown 20 s later after the solution with Ca^{2+} and glutamate was added. Scale bars, 5 μm.

Department of Cell Biology and Department of Pharmacology and Cancer Biology, Box 3709, Duke University Medical Center, Durham, NC 27710, USA.

*To whom correspondence should be addressed. E-mail: tobias@cellbio.duke.edu

We used photobleaching recovery to compare the binding of CaMKII to F-actin and PSD (*9*). Whereas F-actin–localized GFP–β-CaMKII recovered in less than 5 s from a local photobleaching laser pulse (*8*), the fluorescence recovery of PSD-bound GFP–α-CaMKII was longer than 5 min, suggesting that PSD-localized CaMKII is nearly immobile for the duration of glutamate stimulation (Fig. 2B). The same PSD immobilization was observed for GFP–β-CaMKII (*5*). As a control shows (Fig. 2C), cytosolic GFP–α-CaMKII recovered much more rapidly from a local photobleaching pulse. This suggests that the binding of CaMKII to PSD has a much higher affinity than its binding to F-actin.

Because the time required to recruit CaMKII to PSD is important to convert the duration of the synaptic input to the activation of CaMKII targets, we measured the translocation kinetics for CaMKII homo- and hetero-oligomers. Figure 2D shows a series of images used to analyze the translocation time course of GFP–α-CaMKII. The average relative increase in fluorescence intensity at each PSD was plotted as a function of time (*10*). The half-maximal time required for translocation was ~20 s for GFP–α-CaMKII, increased to ~80 s for GFP–α/β-CaMKII hetero-oligomers (1:1 ratio), and was longest (~280 s) for GFP–β-CaMKII (Fig. 2E). In contrast, the dissociation of GFP–β-CaMKII from F-actin was half-completed within 5 s of glutamate addition (Fig. 2F). Thus, dissociation from F-actin is a rapid process, whereas translocation to PSD has a delay time that can be regulated in neurons by the ratio of β- to α-CaMKII subunits in each oligomer.

These measurements define three distinct localization states and two translocation steps of α/β-CaMKII hetero-oligomers. The first rapid translocation step requires a dissociation of β-CaMKII from F-actin, and the second delayed translocation step requires high-affinity binding of α- or β-CaMKII subunits to PSD-localized binding partners. What is the role of these two separate localization states? F-actin and PSD localization states might correspond to the two separate functions of CaMKII in the stabilization of dendritic arbors and synaptic plasticity, respectively. Although potential substrates of F-actin–localized CaMKII are unknown, the function of PSD-localized CaMKII is likely to phosphorylate *N*-methyl-D-aspartate (NMDA) receptors (*11*), AMPA (α-amino-3-hydroxy-5-methyl-4-isoxazolepropionic acid) receptors (*12*), SynGAP (*13*), as well as other PSD-localized substrates involved in synaptic plasticity. Because an earlier study showed that autophosphorylated CaMKII can bind to the NR2B subunit of the NMDA receptor (*14*), this substrate of CaMKII is also a potential candidate for a PSD-binding partner.

In addition to being a substrate and potential binding partner, the NMDA receptor is a Ca^{2+} channel that may itself mediate CaMKII translocation by increasing Ca^{2+} concentration in the postsynaptic terminal. Indeed, the glutamate-induced translocation of GFP–α-CaMKII to PSD was blocked by D-2-amino-5-phosphonovalerate (APV), a selective NMDA receptor blocker (Fig. 3A) (n = 9), suggesting that NMDA receptors are necessary for CaMKII translocation. Furthermore, when NMDA, AMPA, and metabotropic glutamate receptors were selectively stimulated with NMDA, AMPA, and ACPD [*trans*-(1*S*, 3*R*)-1-amino-1, 3-cyclopentanedicarboxylic], respectively, only NMDA induced the PSD translocation of GFP-CaMKIIα (Fig. 3B) (n = 11). This suggests that Ca^{2+} influx through NMDA receptors is

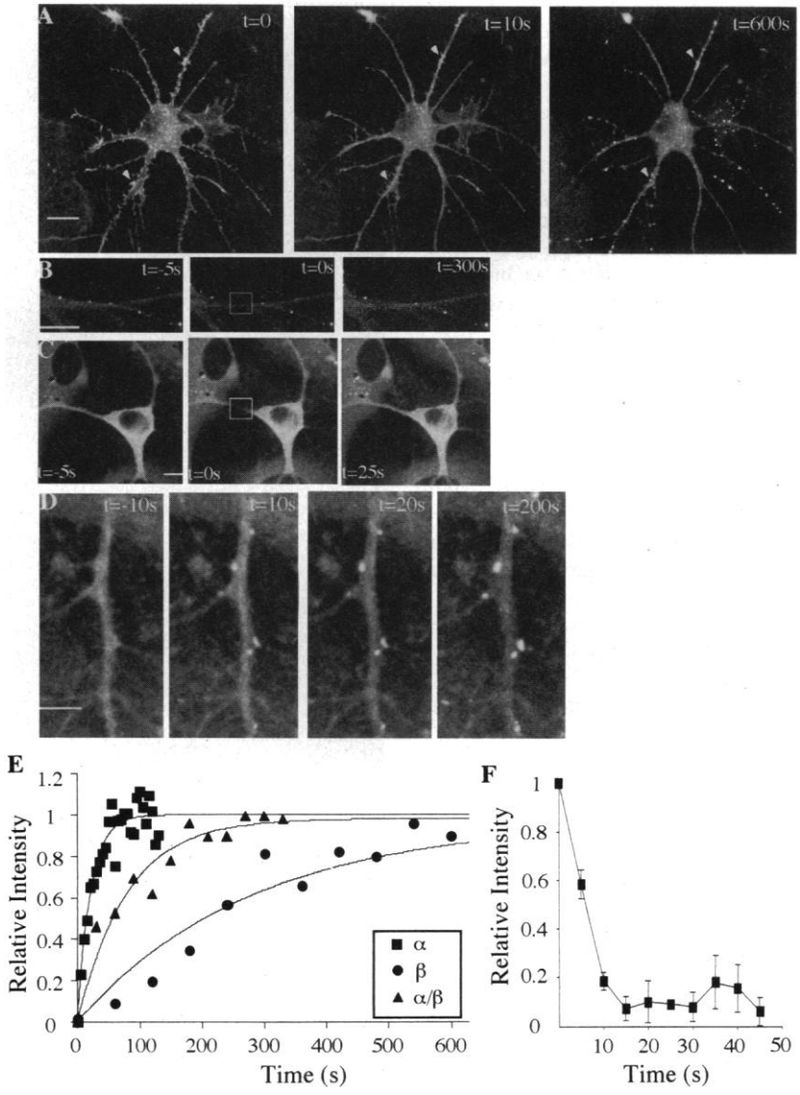

Fig. 2. Differential translocation kinetics of β- and α-CaMKII homo-oligomers and α/β-CaMKII hetero-oligomers. (**A**) Two-step translocation of GFP–β-CaMKII from F-actin to cytosol to PSD. GFP–β-CaMKII–transfected CA3-CA1 neurons showed a localized and filamentous staining pattern reminiscent of the distribution of F-actin (left) (*3*). Stimulation with 100 μM glutamate and 10 μM glycine induced a rapid loss in the F-actin staining pattern (middle). Persistent glutamate stimuli induced a second translocation step to the same punctate pattern observed for CaMKIIα (arrows, right). (**B**) Fluorescence recovery after photobleaching (FRAP) experiments in neurons transfected with GFP–α-CaMKII. The distribution before the photobleaching protocol (left). An individual dendritic site was photobleached 1 min after glutamate addition as indicated by the box in the middle image. Almost no recovery was seen 5 min after photobleaching (right). (**C**) Control measurement, showing rapid recovery of cytosolic GFP–α-CaMKII fluorescence in unstimulated neurons. (**D**) Time course of GFP–α-CaMKII translocation. Glutamate was added at t = 0. (**E**) Time course of PSD translocation of α-CaMKII (square) and β-CaMKII homo-oligomers (circle), and α/β hetero-oligomers (triangle). Half-maximal translocation was 20, 80, and 280 s for α, α/β, and β oligomers, respectively. Traces represent average value of different experiments (n = 12 for α, n = 8 for β, n = 6 for α/β). (**F**) Time course of F-actin dissociation of GFP–β-CaMKII after glutamate addition (n = 6). Scale bars: 10 μm in (A) through (C), and 5 μm in (D).

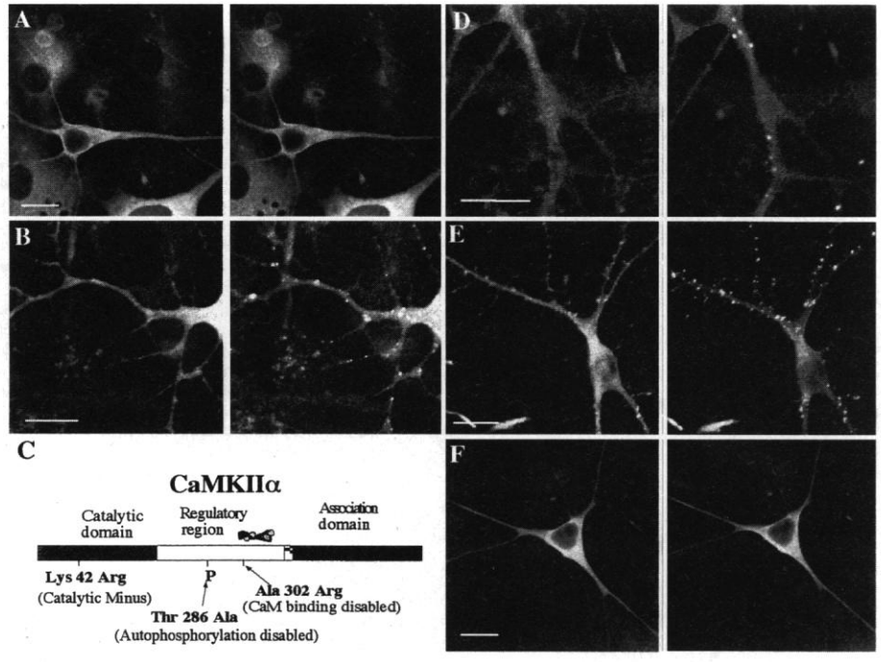

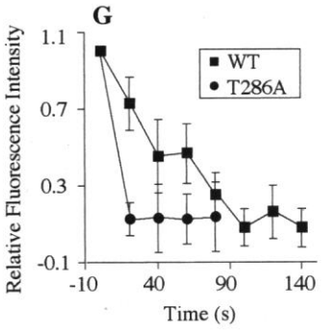

Fig. 3. Regulation of PSD translocation of CaMKII by NMDA receptors, calmodulin-binding, and autophosphorylation. (**A**) PSD translocation does not occur in the presence of the NMDA-receptor blocker APV. Fluorescence images of a GFP–α-CaMKII–transfected neuron are shown before (left) and after (right) glutamate addition in the presence of 300 μM APV. (**B**) Addition of the NMDA-receptor agonist NMDA triggers translocation. Fluorescence images of a GFP–α-CaMKII–transfected neuron are shown before (left) and after (right) addition of 30 μM NMDA. (**C**) Schematic representation of mutant α-CaMKII constructs used for the characterization of the molecular requirements for PSD translocation. (**D**) Glutamate-induced translocation of a catalytically deficient GFP–α-CaMKII to PSD (K42R mutant). Fluorescence images of a neuron transfected with a K42R mutant GFP–α-CaMKII are shown before (left) and ~1 min after (right) addition of 100 μM glutamate and 10 μM glycine. (**E**) Glutamate-induced translocation of an autophosphorylation-deficient GFP–α-CaMKII to PSD [T286A mutant, same protocol as in (D)]. (**F**) A GFP–α-CaMKII mutant deficient in calmodulin binding (A302R) fails to translocate to PSDs [same protocol as in (D)]. (**G**) Potential role of Thr^{286} phosphorylation in delaying the CaMKII dissociation from PSD. Time course of dissociation of GFP–α-CaMKII wild type (WT) (n = 8) and a T286A mutant (n = 8) from PSD. The glutamate solution was exchanged to a low Ca^{2+} solution without glutamate at t = 0. Scale bars, 5 μm.

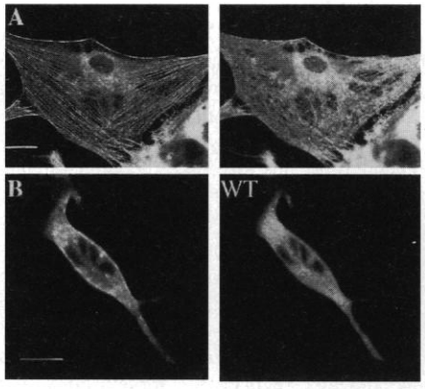

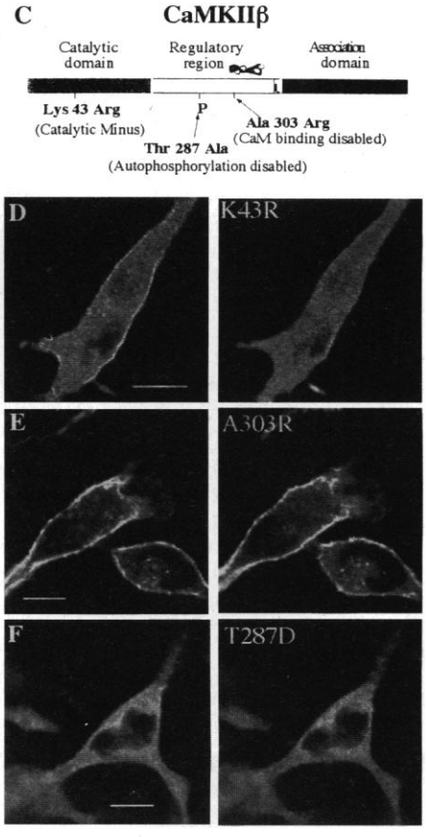

Fig. 4. Dissociation of β-CaMKII from F-actin was triggered by either binding of Ca^{2+}/calmodulin or Thr^{287} autophosphorylation. (**A** and **B**) F-actin dissociation of GFP–β-CaMKII in model cells. (**A**) Hippocampal glial cell transfected with GFP–β-CaMKII showed a distinct stress fiber staining pattern (left). Loss of stress fiber staining pattern 20 s after stimulation with 1 μM ionomycin (right). (**B**) RBL cells transfected with GFP-CaMKIIβ showed a cortical staining pattern reminiscent of the abundant cortical F-actin in these cells (left). Loss of cortical staining after ionomycin stimulation (right). (**C**) Schematic representation of mutant β-CaMKII constructs used for the characterization of the molecular requirements for F-actin dissociation. (**D**) Calcium ionophore induced F-actin dissociation of a catalytic activity–deficient GFP–β-CaMKII (K43R mutant). (Left) Distribution of the mutant before the Ca^{2+} increase. (Right) Distribution 2 min after addition of 1 μM ionomycin. (**E**) A GFP–β-CaMKII mutant deficient in calmodulin binding (A303R) fails to dissociate from F-actin after ionomycin addition. The F-actin prelocalization of this mutant construct is prominently visible in the left and right images. (**F**) A mutant GFP–β-CaMKII with a simulated autophosphorylation at Thr^{287} (T287D) fails to prelocalize to F-actin. The addition of Ca^{2+} ionophore had no apparent effect on the localization of this mutant in the model cells. Scale bars, 5 μm.

not only necessary but also sufficient for PSD translocation.

Which molecular events determine the localization and translocation of CaMKII? Calmodulin binding and autophosphorylation are the two key events in CaMKII activation. Earlier studies showed that NMDA receptor stimuli activate α-CaMKII and trigger autophosphorylation of α- and β-CaMKII (*15*). Autophosphorylation leads to a partially active kinase (*16*) with a several hundred-fold increase in Ca^{2+}-calmodulin–binding affinity (*17*).

CaMKII mutants were used to define the molecular steps of CaMKII translocation (*18*) (Fig. 3C). Because α-CaMKII does not bind F-actin, we used GFP–α-CaMKII instead of hetero-oligomers for the PSD translocation studies. Surprisingly, a kinase-inactive mutant [$Lys^{42} \rightarrow Arg^{42}$ (K42R)] (*19*) still translocated to the PSD, suggesting that kinase activity is not needed for PSD translocation (Fig. 3D) ($n = 7$). Consistent with this result, the autophosphorylation-deficient mutant [$Thr^{286} \rightarrow Ala^{286}$ (T286A)] (*20*) translocated to PSD, showing that autophosphorylation is also not a requirement for PSD translocation (Fig. 3E) ($n = 12$). Furthermore, the $Thr^{286} \rightarrow Asp^{286}$ mutant, which simulates the autophosphorylated CaMKII, did not prelocalize to PSDs (*5*) ($n = 8$). However, when calmodulin binding was disrupted in the $Ala^{302} \rightarrow Arg^{302}$ (A302R) mutant (*21*), no PSD translocation was observed (Fig. 3F) ($n = 6$). This suggests that calmodulin binding, but not autophosphorylation, is necessary and sufficient for PSD translocation.

Even though autophosphorylation does not directly mediate PSD translocation, we determined whether autophosphorylation has an indirect role in PSD translocation by increasing the calmodulin-binding affinity (*17*). The prediction is that such an increase in binding affinity should prolong the association of CaMKII with PSD after a transient Ca^{2+} increase. Indeed, when the neuronal Ca^{2+} concentration was lowered by removing external glutamate and Ca^{2+}, the autophosphorylation-deficient T286A mutant dissociated much more rapidly from PSD compared to the wild type (Fig. 3G). This finding adds a new perspective to the earlier suggestion that autophosphorylation is necessary for binding of CaMKII to PSD (*6*) or NMDA receptors (*14*). In the new model, autophosphorylation of CaMKII may function as a short-term biochemical "memory" by prolonging the localization of active CaMKII near its site of action.

We then explored the molecular requirements for β-CaMKII dissociation from F-actin, using model cells that contain F-actin but lack the PSD translocation event. Actin localization of GFP–β-CaMKII can be readily visualized in glial cells, which are rich in actin stress fibers (Fig. 4A, left), and in rat basophilic leukemia (RBL) cells, which are rich in cortical actin (Fig. 4B, left). The F-actin localization of β-CaMKII was lost after an increase in Ca^{2+} concentration (Fig. 4, A and B; right) ($n = 25$).

We tested the β-CaMKII mutants (Fig. 4C) in the RBL cell model. The kinase-deficient GFP–β-CaMKII mutant (K43R) showed prelocalization and dissociation similar to wild-type GFP–β-CaMKII, suggesting that kinase activity is not required for F-actin dissociation (Fig. 4D, $n = 14$). A GFP–β-CaMKII deficient in calmodulin binding (A303R) bound effectively to F-actin and failed to dissociate after an increase in Ca^{2+} concentration (Fig. 4E, $n = 16$). Consistent with this result, W-7, a calmodulin antagonist, also blocked the dissociation of GFP–β-CaMKII from actin cytoskeleton (*5*). However, no F-actin localization was observed when Thr^{287} was replaced by aspartic acid (T287D), even in the absence of an increase in Ca^{2+} concentration (Fig. 4F, left) ($n = 18$). This suggests that either Ca^{2+}-calmodulin–binding or autophosphorylation at Thr^{287} are both sufficient to induce the dissociation of β-CaMKII from F-actin. These measurements define a separate cytosolic autophosphorylated state of CaMKII which cannot translocate to PSD unless calmodulin is bound.

We demonstrate the existence of distinct molecular states of α- and β-CaMKII, corresponding to an F-actin–bound, a cytosolic, and a PSD-bound form of the hetero-oligomeric kinase. Whereas calmodulin binding or autophosphorylation of β-CaMKII were both sufficient for the dissociation of CaMKII from F-actin, PSD translocation of CaMKII required the binding of calmodulin to α- or β-CaMKII. Because autophosphorylation induces a several hundred-fold increase in calmodulin-binding affinity (*17*), a role for autophosphorylation of α- or β-CaMKII is to delay calmodulin dissociation and thereby prolong the stimulus-induced CaMKII localization to PSD. Thus, two molecular events—calmodulin binding and autophosphorylation—are not only used to control CaMKII enzyme activity but also to dynamically regulate the translocation and localization of CaMKII with its cytoskeletal and synaptic target sites.

References and Notes

1. R. Malinow, H. Schulman, R. W. Tsien, *Nature* **335**, 820 (1988); D. L. Pettit, S. Perlman, R. Malinow, *Science* **266**, 1881 (1994); S. Glazewski, C.-M. Chen, A. Silva, K. Fox, *ibid.* **272**, 421 (1996); J. A. Gordon *et al.*, *Neuron* **17**, 491 (1996); M. Mayford *et al.*, *Science* **274**, 1678 (1996); M. Mayford *et al.*, *Cell* **81**, 891 (1995); A. J. Silva, S. Tonegawa, C. F. Stevens, Y. Wang, *Science* **257**, 201 (1992).
2. G.-Y. Wu and H. T. Cline, *Science* **279**, 222 (1998).
3. CA3-CA1 hippocampal cultures (postnatal day 2 to 4) were prepared as previously described (*8*). Neurons, 6 to 14 days in culture, were transfected by microelectroporation of the respective mRNA or of mixtures of different mRNAs (*22*). For some of the mutants, DNA constructs were used instead of the mRNA. Three electrical pulses (20 V/mm, 20 s apart) were applied to the neurons immediately after mRNA or DNA application. Localization and translocation studies were done 8 to 16 hours after transfection.
4. Supplementary figures can be found at the *Science* Web site (www.sciencemag.org/feature/data/986549.shl)
5. K. Shen and T. Meyer, data not shown.
6. S. G. Miller and M. B. Kennedy, *J. Biol. Chem.* **260**, 9039 (1985); S. M. Shields *et al.*, *J. Neurochem.* **43**, 1599 (1984); J. R. Goldenring, *ibid.* **42**, 1077 (1984); B. R. Hu and T. Wieloch, *ibid.* **64**, 277 (1995); T. Suzuki *et al.*, *ibid.* **63**, 1529 (1994); S. Strack *et al.*, *J. Biol. Chem.* **272**, 13467 (1997); Y. Yoshimura and T. Yamauchi, *ibid.*, p. 26354.
7. Fluorescent images were taken at an excitation wavelength of 488 nm, using a confocal microscope (LSM410, Zeiss Inc.). For the immunocolocalization experiments, neurons were fixed with methanol for 10 min at −20°C and blocked with bovine serum albumin (10 mg/ml). Monoclonal antibody to PSD-95 (1:200) was used (Affinity Bioreagents), followed by Cy5-labeled secondary antibodies. Cy5 distribution was monitored by excitation at 568 nm.
8. K. Shen *et al.*, *Neuron* **21**, 593 (1998).
9. For photobleaching experiments, the microscope was zoomed onto a small region of the neuron at maximal laser power. Recovery of the fluorescence was then measured at lower laser power by sequential imaging of the entire neuron.
10. The translocation time course of α-, β-, and α/β-CaMKII oligomers to PSD was determined by taking series of 50 to 100 images of neurons after glutamate addition. The local increase in fluorescence intensity at PSD sites was then determined by sequentially measuring the average fluorescence intensity in a small box around these sites and by determining $(I_{PSD} - I_{AV})/I_{AV}$. Each of the traces shown was calculated from an average of such intensity recordings. The same type of analysis was also used to measure the time course of dissociation of β-CaMKII from F-actin after glutamate addition. The average intensity was measured in small cortical regions instead of the PSD.
11. V. Ramakrishnapillai *et al.*, *J. Biol. Chem.* **271**, 31670 (1996).
12. E. McGlade-McCulloh *et al.*, *Nature* **362**, 640 (1993); A. Barria, D. Muller, V. Derkach, L. C. Griffith, T. R. Soderling, *Science* **276**, 2042 (1997).
13. H. Chen *et al.*, *Neuron* **20**, 895 (1998).
14. S. Strack and R. J. Colbran, *J. Biol. Chem.* **273**, 20689 (1998); F. Gardoni *et al.*, *J. Neurochem.* **71**, 1733 (1998).
15. K. Fukunaga, T. R. Soderling, E. Miyamoto, *J. Biol. Chem.* **267**, 22527 (1992).
16. C. M. Schworer, R. J. Colbran, T. R. Soderling, *ibid.* **261**, 8581 (1986); L. L. Lou, S. J. Lloyd, H. Schulman, *Proc. Natl. Acad. Sci. U.S.A.* **83**, 9497 (1986).
17. T. Meyer, P. I. Hanson, L. Stryer, H. Schulman, *Science* **256**, 1199 (1992).
18. GFP-tagged α- and β-CaMKII isoforms were characterized previously (*8*). Point mutations of α- and β-CaMKII were created using polymerase chain reactions in the in vitro translation vector pSHIRO3 (*22*).
19. P. Hanson *et al.*, *Neuron* **12**, 943 (1994).
20. Y. L. Fong *et al.*, *J. Biol. Chem.* **264**, 16759 (1989); P. Hanson *et al.*, *Neuron* **3**, 59 (1989).
21. S. Mukherji and T. R. Soderling, *J. Biol. Chem.* **269**, 13744 (1994).
22. M. F. Teruel and T. Meyer [*Biophys. J.* **73**, 1785 (1997)] described the microporation technique; H. Yokoe and T. Meyer [*Nature Biotechnol.* **14**, 1252 (1996)] described the RNA transfection technique; M. F. Teruel *et al.* (in preparation) described the efficiency of RNA cotransfection in neurons.

23. We thank B. Wang for support with the neuronal culturing, K. Subramanian for molecular biology support, and M. Teruel for developing the neuronal RNA transfection technique. We also thank E. Oancea, W. Chen, and A. Means and M. Teruel for stimulating discussions. Supported by NIH grant GM-48113.

17 November 1998; accepted 3 March 1999